Model Submarine Sail Geometry Optimisation – A Numerical and Experimental Investigation

Jeremy Wotherspoon[1], Ahmed Swidan[2], Warren Smith[3], Alaa Osman[4]
1 SBLT, UNSW Canberra at ADFA, Australia j.wotherspoon@student.unsw.edu.au
2 UNSW Canberra at ADFA, Australia a.swidan@unsw.edu.au
3 UNSW Canberra at ADFA, Australia w.smith@adfa.edu.au
4 UNSW Canberra at ADFA, Australia a.osman@adfa.edu.au

Abstract
This paper aims to address improvements to the current model of the Subs in Schools (SiS) Technology Challenge, with a focus on the redesign and improvement of a model submarine's sail. The sail is an important feature with regards to resistance as it contributes disproportionately to total resistance, thus affecting required power and subs' endurance. A series of wind tunnel experiments were conducted at the University of New South Wales Canberra, in order to benchmark a range of model sails. This benchmarking data was utilised to validate RANS (Reynolds-averaged Navier–Stokes equations) Computational Fluid Dynamics (CFD) simulations using ANSYS™. The validated numerical simulations were conducted to investigate the influence of different design variables being; slenderness ratio, bluntness ratio and the maximum frontal cross-section area on sail resistance in order to optimise the geometry within the dimensional constraints provided by SiS technology challenge. The computed results were in good agreement with the measured data and provided insight to the effect of submarine sail geometry design variables on resistance. An educational package on the effect of these design variables on the drag were provided to the SiS students. This would allow students to perform further investigations to enhance the hydrodynamic performance of the SiS model.
This paper reflects a work in progress as part of a 2019 undergraduate honours project conducted by the lead author.

Nomenclature

P	Density (kg/m^3)	L	Total length of model (m)
μ	Kinematic viscosity on model (m^2/s)	R	Total resistance (N)
A_W	Wetted area surface (m^2)	R_F	Frictional resistance (N)
C_D	Total resistance coefficient	R_{VP}	Viscous pressure resistance (N)
C_F	Frictional resistance coefficient	Re	Reynolds number
C_{VP}	Viscous pressure resistance coefficient	V	Speed of model (m/s)

Introduction
Small scale submarine models exist primarily for the purpose of research with the goal to provide advancements to full scale submarines. The common methods of testing the submarine models are as follows: seakeeping experimental tests using towing tank, wind tunnel or numerical simulations. The most noteworthy example being the first substantial submarine model tests, the Gertler streamline bodies experiments from 1950 (Gertler, 1950), which resulted in the development of "tear drop" shaped hulls first introduced on the USS Albacore in 1958. This research greatly improved the understanding of flow around submerged bodies and resistances in submarine design.

However, Re-Engineering Australia (REA) produced a program piloted in 2014, namely: the Subs in Schools (SiS) Technology Challenge that exists to increase interest in STEM fields in general and to introduce students to the engineering challenges related to submarines and underwater vehicles. The current model of SiS has teams assemble a submarine model, with more focus on providing coding, producing engineering drawings and debugging issues that occur throughout the process. The concept within this paper is to address a previously un-addressed field of potential within the SiS technology challenge being resistance. This investigation into resistance will provide the students an understanding of fluid flow, addressing areas for improvement, such that they can re-design parts to improve their model's performance. Overall increasing their engineering knowledge and the experiences gained within the competition.

This research uses a model submarine sail as a case study such to optimise a component of the model within the guidelines of the competition. This is to demonstrate potential areas of improvement and add knowledge to the teams on how to approach hydrodynamic improvements of the model. In this paper, CFD simulations are utilised with the purpose of estimating the hydrodynamic performance characteristics, e.g. drag and lift coefficients, velocity vectors and the pressure contours around the model submarine' sail. The methods reported in this paper are the pre-processing RANS based CFD simulations including detailed grid-independence study to provide confidence in the computed results The CFD simulations were employed to analyse the influence of 3 design parameters being; slenderness ratio, bluntness ratio and the maximum frontal cross-section area between 3 varying geometries, such to find the optimal values of these design variables in order to achieve a minimal drag force for a given sail volume.

This case study and the processes involved were performed to understand what is required to perform hydrodynamic improvements on submarine model components. The process, results, summary and knowledge gained will provide useful and detailed information to the students on factors affecting resistance and hydrodynamic performance which they can use to perform improvements within SiS.

Sail Design

The largest appendage and a significant contributor to overall drag with estimates of up to 30% of total resistance is the sail (Friedman, 1984). The sail has many key features when it comes to submarine operations such as "stowage and support for the masts when raised, a conning position when in harbour for berthing, safe transfer to the open deck at sea without swamping, underwater handling stability, and an ability to operate covertly while submerged at shallow depth" (Joubert, 2004). Therefore, the sail can be seen as a key feature affecting both operational factors and performance. Submarine sail design is a fine balance with regards to height, too short and submarine speed will be restricted when using masts. However, if it is too tall or too thin the snap roll will cause excessive forces on the sail and risk damage to the hull, masts and other sensitive components housed within the sail (Hervey and Till, 1994).

Flow Resistance of the Submarine Sail

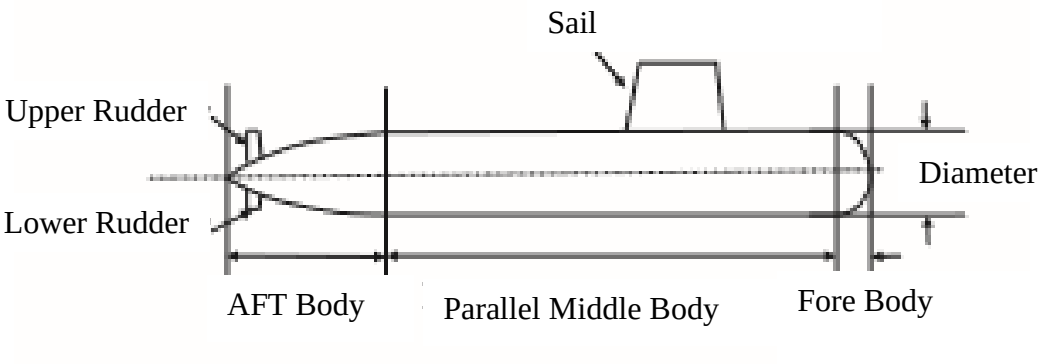

Figure 1. Side view of a generic submarine hull (Renilson, 2015).

When discussing resistance of any component of a deeply submerged submarine it can be thought of as two components; friction resistance and form resistance, wave resistance can be neglected due to the deep submersion (Bertram, 2012). Submarines are designed to operate in submerged conditions as that is their primary area of operation, at depth there is no wave making and also for snorkeling at low speed wave resistance is also negligible.

$$C_D = \frac{R}{0.5\rho A_W V^2}$$ … Equation 1. Total resistance coefficient (Moonesun, *et al*. 2014).

$$C_F = \frac{R_F}{0.5\rho A_W V^2}$$ … Equation 2. Frictional resistance coefficient (Moonesun, *et al*. 2014).

$$C_{VP} = \frac{R_{VP}}{0.5\rho A_W V^2}$$ … Equation 3. Viscous pressure resistance coefficient (Moonesun, *et al*. 2014).

Despite the not ideal nature of a sail on a submarine as can be seen by the non-streamline nature of the sail as seen in Figure 1. However, the large appendage in one form or another is necessary for any modern conventional submarine, as it acts as the bridge conning position and the housing for various periscopes, masts and ducting (Bertram, 2019). Idealised hydrodynamics would suggest that if the sail must exist it should be as thin as possible to reduce drag as described in equation 3. This being the viscous pressure equation for a bare hulled submarine however the theory still applies to just the sail (Moonesun, *et al*. 2014).

Viscous pressure resistance is due to the sail inducing local flow fields with different velocities than the average, this results in an increase in shear stresses and increased energy losses in the boundary layer. This form of resistance is minimised by having a length where the sections vary by small increments along the sail. Also, when considering frictional resistance as described in equation 2, this still is valid when solely considering the sail as this form of resistance is cause by viscous shear of water over the surface (Bertram, 2019). This is fundamentally reduced by causing a reduction in wetted surface, therefore for a given volume a sphere would be the ideal shape to achieve this, however a spherical sail produces its own problems, this being an increase in the form resistance. Therefore, the two forms of resistance for submarines and their optimal solutions contradict one another, as demonstrated in Figure 2.

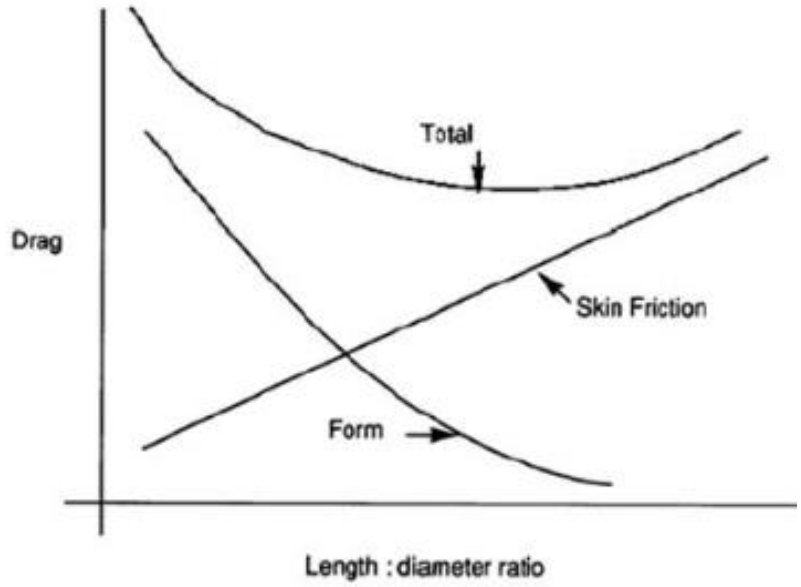

Figure 2. Graph displaying the contradicting nature of form and frictional drag (Moonesun *et al*., 2013).

Thus, the main areas of focus in the study of sail optimisation is with the interference drag between the hull and the sail, and location of the sail along the length of the hull as these interactions have the largest part to play. However, the flow around the geometry of the sail itself is still of notable effect due to the sail's large contribution to total resistance, a flow simulation of a maneuvering submarine can be seen in Figure 3, demonstrating flow interference caused by the sail. Recommendations for sail design exist, in order to minimise skin friction drag, the sail should be kept as small and smooth as possible (Mises, 2012). Pressure drag is minimised by streamlining of the shape, with maximum thickness being approximately 45% of length and thickness to length ratio should not exceed 12.5%.

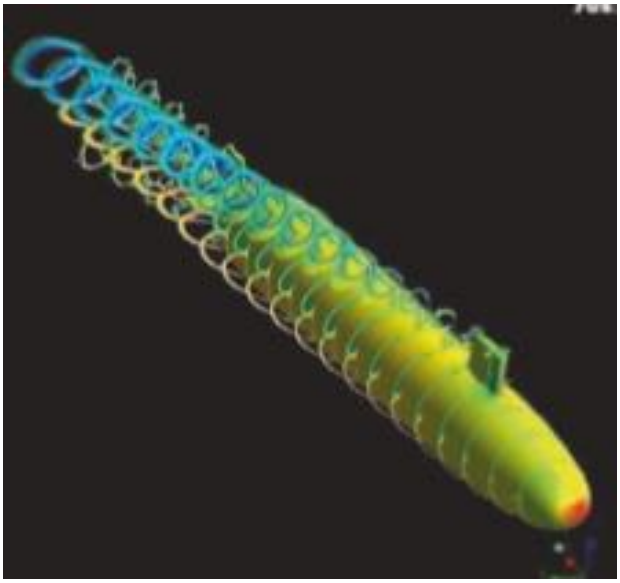

Figure 3. Flow vortices around a maneuvering submarine (Renilson, 2015).

Design of Experiments (DOE): Geometries

For the both CFD and experimental processes various simplified sail geometries were generated within the constraints of the SiS technology challenge, being the sail must be longer than 100mm, must be wider than 30mm and must have a height of at least 50mm (REA, 2019). A simplified sail geometry was utilised such to ignore the transition region addressed in other optimisation studies. These geometries were formed and evaluated using 3 design variables, these being a length to width ratio (slenderness ratio), a width to frontal radius ratio (bluntness ratio) and a height by width (maximum frontal cross-section area). Geometries are detailed in table 1 and 2 and displayed in Appendix A.

Table 1: Primary Sail Geometric Parameters

Sails: Volume 'V'(mm^3)	**Length 'L'(mm)**	**Width 'W'(mm)**	**Frontal Radius 'FR'(mm)**	**Height 'H'(mm)**
1: 2.1027e+05	200	30	20	60
2: 2.1027e+05	127	50	30	56
3: 2.1027e+05	159	40	70	51

Table 2: Sail Design Variables

Sails: Surface Area 'SA'(mm^2)	**Slenderness Ratio 'SR'**	**Bluntness Ratio 'BR'**	**Maximum frontal cross-section area 'FCSA'(mm^2)**
1: 32118	6.66666	1.5	1800
2: 23656	2.54	1.66666	2800
3: 25408	3.975	0.57143	2040

CFD Simulations

Modelling for CFD Simulations

The modelling of the geometries was done using the inbuilt geometry modeler within ANSYS-FLUENT. The geometry itself was created through the use of a sketch of an ellipse as the front of the sail, a semi-circle as the tail and two connecting lines. This sketch was then extruded to form a geometry. Which was removed from an enclosure being the wind tunnel of overall geometry with a length of 900mm, with a width and height of 460mm.

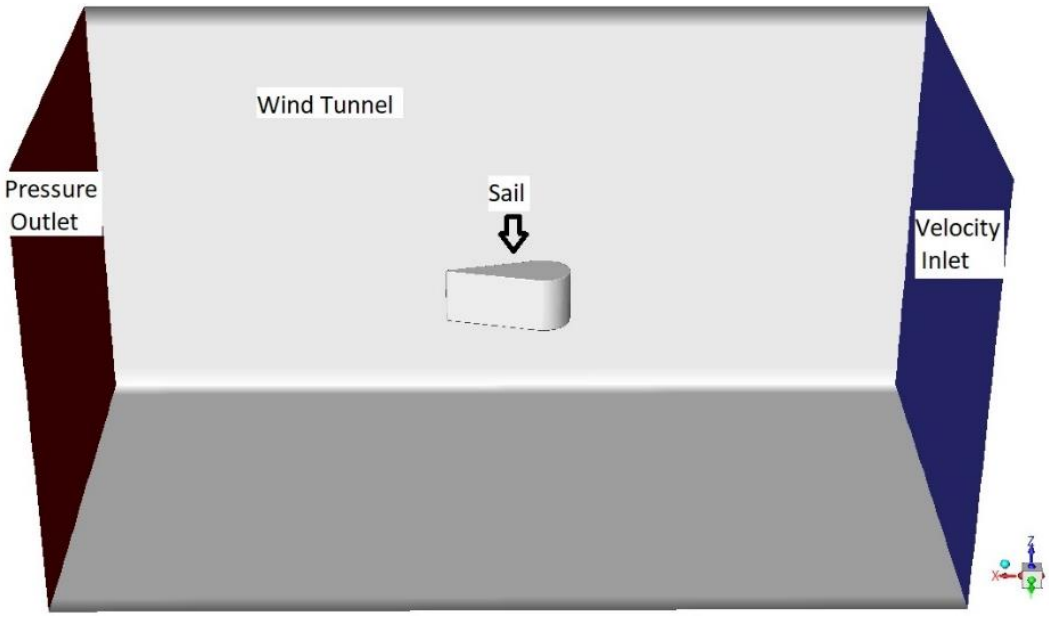

Figure 4: Display of basic setup (Front walls of wind tunnel removed for visualisation)

This removal of the sail was done using a Boolean subtraction operation, such that the sail itself was not analysed, but the flow around the surface was. This subtracted geometry was meshed within the ANSYS-FLUENT in-built meshing tool. The modelling physics were setup in ANSYS-FLUENT setup, the input information is based on an approximate movement velocity of the submarine modelled at three different velocities being, 0.75m/s, 1m/s and 1.25m/s displayed in figure 4. The speed induces a laminar flow around the sail geometry, with Reynolds number calculations detailed in Appendix B.

Independent Mesh Investigation

The independent mesh investigation undertaken involved the comparison of 3 different mesh sizes, meshed under the same conditions in order to verify an appropriate size mesh to use for the simulations. This was done with respect to the variation in drag, the number of elements, therefore computational time. The analysed geometry for this mesh investigation was geometry 2 as it has the smallest surface area and therefore with the primary focus of the mesh being on retaining the geometry and analysis on the geometry itself, a smaller surface area plays the largest role in reducing the number of elements. Proximity and curvature sizing functions were used so the sail curves maintained their curvature and smoothness and the proximity allowed the flow directly around the sail to be more accurately captured. The meshing method applied to the geometry was a multi zone mesh due to the massive variation in the geometry surface and the far field. A prism mapped mesh type with a pave surface mesh method was used for the semi-structured mesh on the sail such to retain the sail edges and curvature at the front and rear of the sail. A tetra/pyramid free mesh type was used so that the fine prism inflation layer could be applied. The inflation layer consists of 10 layers with a growth rate of 1.1 and a first layer thickness of 1E-05. The various number of elements for the different mesh qualities are detailed in table 3, with their effect on the total drag for the same continuity.

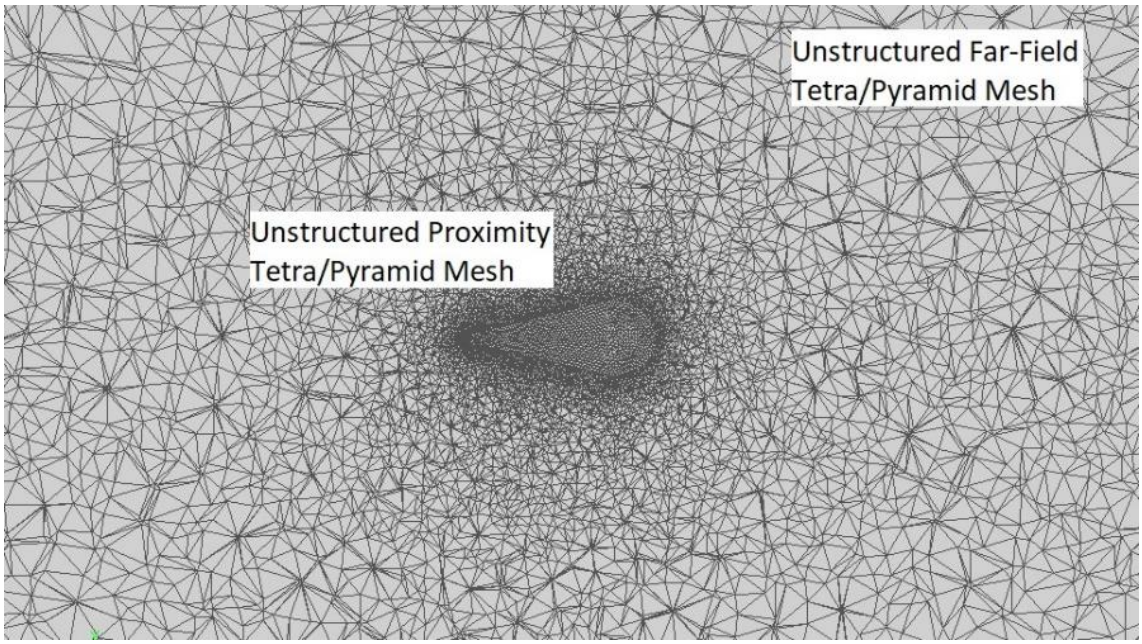

Figure 5: (a) Top view of whole mesh (Medium Mesh)

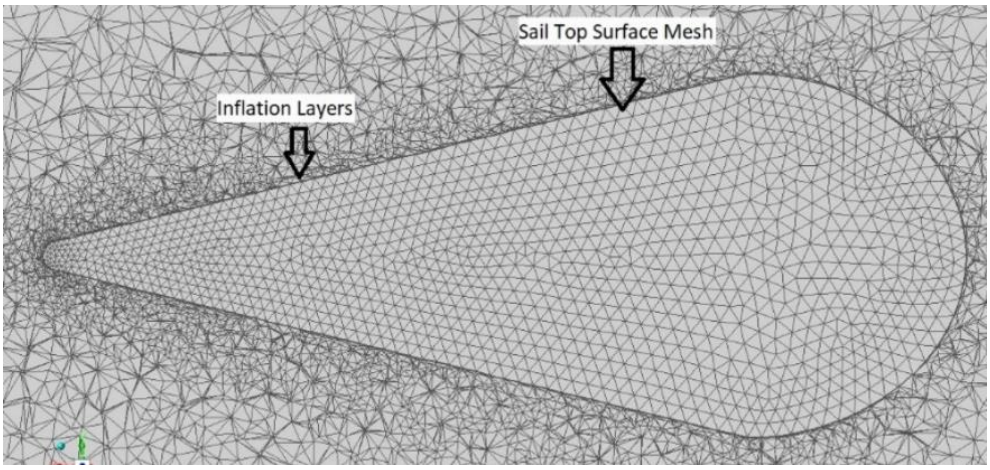

Figure 5: (b) Top view of sail mesh and inflation layers (Medium Mesh)

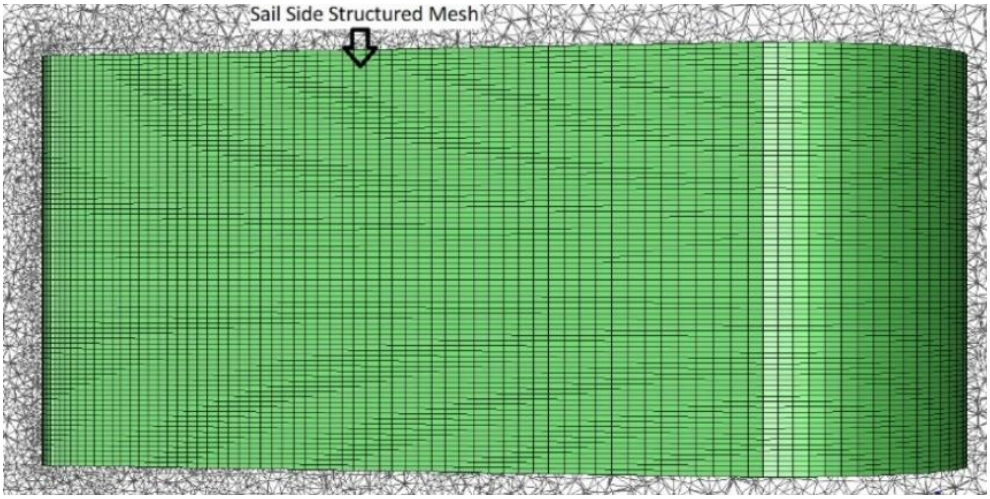

Figure 5: (c) Side view of sail structured mesh (Medium Mesh)

Table 3: Independent Mesh Analysis Results

Fineness of Mesh 2	Elements	Nodes	Comparison Continuity	Total Drag (N)	Variation (%)
Course	617825	206876	4.93E-04	0.70103	
Medium	797387	267492	4.89E-04	0.45686	-34.83
Fine	1405492	450138	4.95E-04	0.44586	-2.41

The results of the independent mesh investigation as detailed in table 2, displayed the variation from the course to the medium mesh provides a variation of the drag value of -34.83% for an element increase of 179562. However, the increase from medium to fine provides a drag variation of -2.41% for an element increase of 608105. For maintaining the same meshing format and respective mesh quality the medium mesh was deemed feasible with respect to the variation in drag for the number of elements present.

Procedure for CFD Analysis

The CFD analysis module provided within ANSYS-FLUENT is a simple set up solver, however in order to achieve accurate and stable solutions is more difficult. This module provides the ability to control relaxation factors to aid with convergence rates and stability of solutions. The simulations were performed using laminar flow and energy equations, with the simple scheme method of pressure-velocity coupling.

The gradient method used was least squares cell based, pressure equation was second order, momentum equation first order upwind and energy equation second order upwind. With the under-relaxation factor controls primarily set to default conditions.

The required convergence was 1e-04, being loosely converged for the simulations as this allows the difference in results to be clearly illustrated between the geometries and can be easily achieved for all geometries either using default controls or through minor manipulations of relaxations factors. To achieve this level of convergence it typically required approximately 220 iterations being for geometry 2 and 3 whereas geometry 1 required manipulation of relaxation factors. All simulations were run for at least 500 iterations passed required convergence to ensure the stability of solution.

CFD Results

The numerical values from the CFD solution are listed in tables 4, 5 and 6. Table 4 details the pressure including pressure drag, table 5 details the velocity including x-directional velocity and table 6 provides an overall drag summary.

Table 4: (a) Pressure Results for Sail 1

Velocity (m/s)	Minimum Pressure (Pa)	Maximum Pressure (Pa)	Pressure Difference (Pa)	Pressure Drag (N)	Pressure Drag Variation (%)
0.75	-929.46	291.26	1220.7	0.10200	
1	-1655.0	516.80	2171.8	0.18086	77.301
1.25	-2592.0	806.53	3398.5	0.28267	56.291

Table 4: (b) Pressure Results for Sail 2

Velocity (m/s)	Minimum Pressure (Pa)	Maximum Pressure (Pa)	Pressure Difference (Pa)	Pressure Drag (N)	Pressure Drag Variation (%)
0.75	-825.45	286.982	1112.4	0.23088	
1	-1463.6	509.23	1972.9	0.40920	77.230
1.25	-2288.1	794.77	3082.9	0.63860	56.061

Table 4: (c) Pressure Results for Sail 3

Velocity (m/s)	Minimum Pressure (Pa)	Maximum Pressure (Pa)	Pressure Difference (Pa)	Pressure Drag (N)	Pressure Drag Variation (%)
0.75	-862.13	289.54	1151.6	0.094154	
1	-1537.4	513.57	2051.0	0.16665	77.001
1.25	-2409.3	801.28	3210.6	0.26000	56.015

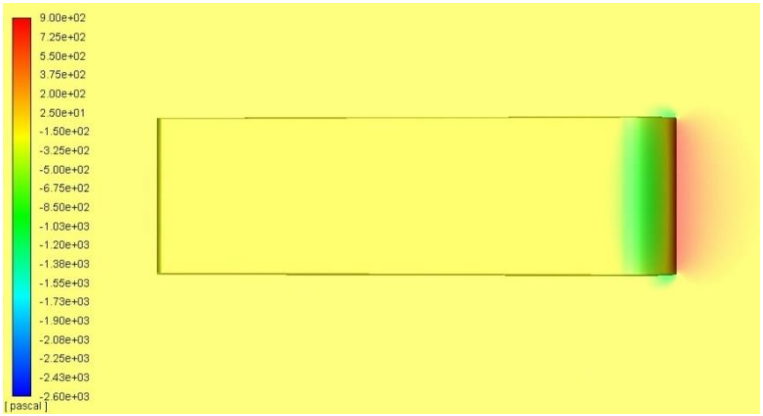

Figure 6: (a) Contours of static pressure geometry 1 at 1.25m/s, side view

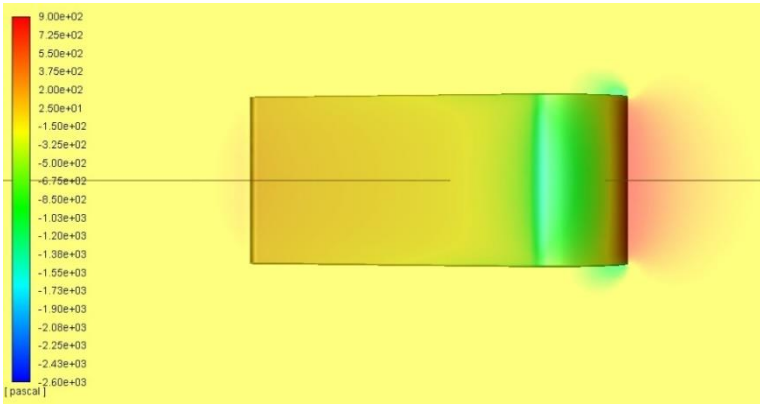

Figure 6: (b) Contours of static pressure geometry 2 at 1.25m/s, side view

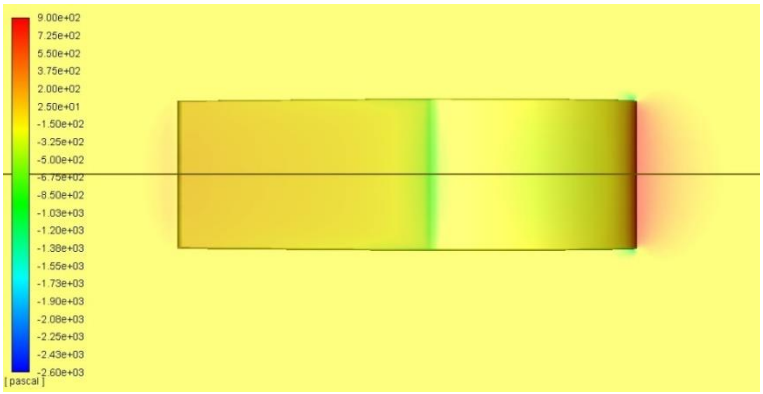

Figure 6: (c) Contours of static pressure geometry 3 at 1.25m/s, side view

The contours of static pressure around the 3 geometries, are provided for the inlet velocity of 1.25m/s, in figure 6. The colour maps of the 3 geometries in figure 6 are all scaled from -2600Pa (dark blue) to 900Pa (Red) for the 1.25m/s, this allows for effective comparison between the different geometries.

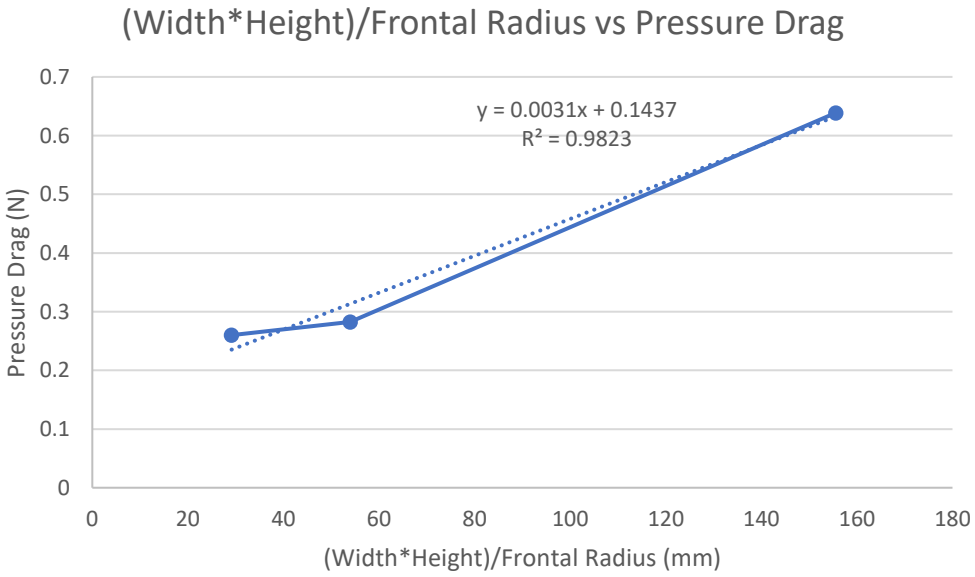

Figure 7: Graph of primary features of the geometries and the influence on the pressure drag at 1.25m/s.

When comparing the maximum and minimum pressures as well as the pressure drag between the various geometries, the design variables and their influence must be considered as well as the response to velocity variations. Figure 6 displays that the static pressure is mainly influenced by the frontal region of the sail. This is dictated by primarily by design variables of bluntness ratio and the maximum frontal cross section.

All other velocities and corresponding pressure drag values, exhibit similar R^2 when approximated with a linear fit. This demonstrates the direct relationship between a high width and height and an increased pressure drag value, however this effect can be greatly reduced through having a larger frontal radius, as despite having the second largest maximum frontal cross-sectional area it has the lowest pressure drag value. This demonstrated in figure 6 (c), as there is a sharp pressure increase at the very front of the sail, however the variation in pressure is spread across the length of the frontal radius thus reducing the pressure drag. In contrast figure 6 (a) and (b) the pressure changes rapidly over a short distant as demonstrated by their high bluntness ratio, causing much greater pressure changes especially visible in figure (b) with the highest bluntness ratio. Also, as the inlet velocity increases the variation in pressure drag reduced significantly, this suggests that if a faster velocity could be achieved the magnitude of the drag would increase but the relative effect would decrease.

Table 5: (a) Summary of velocity results for sail 1

Velocity (m/s)	Maximum Velocity (m/s)	Maximum x- axis Velocity (m/s)	Minimum x- axis Velocity (m/s)	Viscous Drag (N)	Viscous Drag Variation (%)
0.75	1.0653	0.99757	-0.82608	0.062760	
1	1.4738	1.3345	-1.2336	0.090060	33.775
1.25	1.8907	1.6713	-1.6799	0.11853	25.237

Table 5: (b) Summary of velocity results for sail 2

Velocity (m/s)	Maximum Velocity (m/s)	Maximum x- axis Velocity (m/s)	Minimum x- axis Velocity (m/s)	Viscous Drag (N)	Viscous Drag Variation (%)
0.75	1.1668	1.1405	-0.58954	0.033373	
1	1.6326	1.5332	-0.83681	0.047497	34.425
1.25	2.1548	1.9255	-1.1137	0.062566	25.58

Table 5: (c) Summary of velocity results for sail 3

Velocity (m/s)	Maximum Velocity (m/s)	Maximum x-axis Velocity (m/s)	Minimum x-axis Velocity (m/s)	Viscous Drag (N)	Viscous Drag Variation (%)
0.75	1.4853	0.94838	-1.4330	0.050828	
1	1.6659	1.2875	-1.5572	0.072715	35.76
1.25	2.2330	1.6262	-1.7257	0.096143	26.31

Table 6: Summary of Drag forces of three sail configurations, namely 1, 2 and 3, at 1.25m/s

Sail	Viscous Drag (N)	Pressure Drag (N)	Total Drag (N)
1	0.11853	0.28267	0.4012
2	0.062566	0.63860	0.701166
3	0.096143	0.26000	0.356143

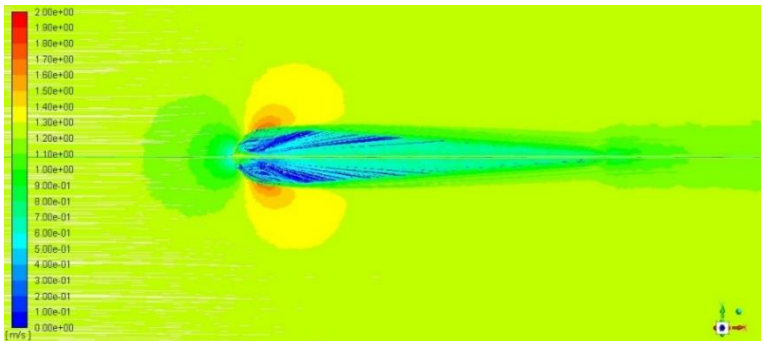

Figure 8: (a) Velocity path lines around geometry 1 at 1.25m/s, top view

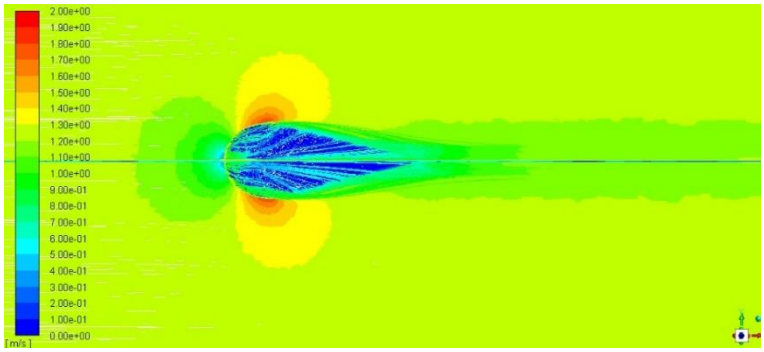

Figure 8: (b) Velocity path lines around geometry 2 at 1.25m/s, top view

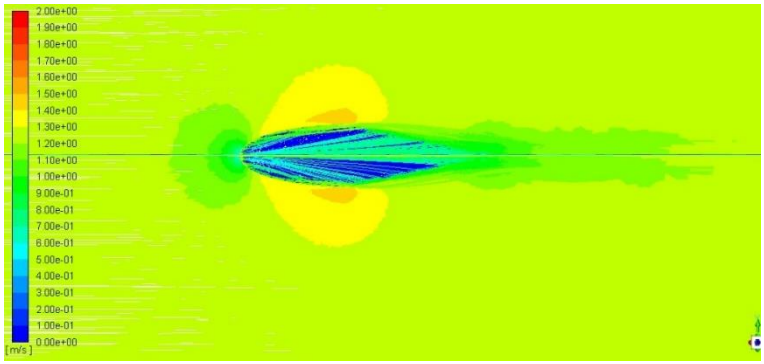

Figure 8: (c) Velocity path lines around geometry 3 at 1.25m/s, top view

The velocity path lines around the 3 geometries, are provided for the inlet velocity of 1.25m/s, in figure 8. The colour maps of the 3 geometries in figure 8 are all scaled from -0m/s (dark blue) to 2m/s (Red), this allows for effective comparison between the different geometries. Figure 8 a, b and c illustrate the region of maximum velocity for all sails is slightly away from the surface itself and just downwind of the widest point of the sail. This is what can be expected with reference to figure 6 also as this is the region of lowest pressure on the sail, allowing the flow to move more easily from high to low pressure.

A key region within figure 8 is downwind of the tail, with the darker inconsistent region due to the effects of wake. Wake plays a large effect in the calculation and the effect of drag on an object. It can be seen from the size of the wake fields, that they interact as a type of pressure, which is also represented in table 5 along with the x-axis velocities, the negative x-axis velocity indicates there are significant wake vortices. As with any form of pressure drag as previously discussed it can be reduced by minimising the changes in geometry over a given length, being a traditional aerodynamic shape, with a long frontal radius, small

width and height and a length such that it has the required volume for its purpose. Viscous drag, as can be seen in table 5 and 6 is only a small contributor to total drag however on this scale and at these velocities it is still significant and can easily become more so as surface roughness and external features come into play. However, viscous drag is primarily a feature of surface area as described in equation 2 previously.

The highest performing sail as described within table 6 was sail 3, as it had the lowest drag for the given volume. Sail 3 did not have the smallest width, length or surface area; however, it did have the smallest bluntness ratio due to its large frontal radius. As has been examined through the static pressure contours and velocity path lines the effect of the large frontal radius in slowly dissipating the pressure is of significance to a sails performance.

Conclusion

In this paper, a series of submarine sails have been numerically modelled, and analysed using ANSYS-FLUENT. The drag characteristics of these isolated sail geometries were compared with respect to the individual static pressure contours and velocity path lines of the geometries. The pressure drag, viscous drag and total drag measurements were taken at 3 different velocity points on 3 geometries with variations in chosen design variables such to achieve a minimal drag for a constant volume. The findings detail the significance of a frontal radius in minimising pressure drag. Where possible width and height should be reduced such to reduce maximum frontal cross-section and bluntness ratio and thus increasing the slenderness ratio, however these have constraints both within the SiS technology challenge and in real life operational considerations. Surface area also contributes with respect to the viscous drag, although only a small component of the total drag it is still of concern in terms of optimisation. Although, these series of simulations and corresponding results are currently without validation, however they stand in agreement with the theory expected and accurately represent the physics of the sail.

Future Work

This is an ongoing project and still requires further work on the topics of validation which will be achieved through conducting series of experiments utilizing a sub-sonic wind tunnel facility using three dimensional models of the presented geometries. The knowledge gained from the current simulations will go into further work to extend to an optimisation of this geometry within the predefined constraints. This extension will in further detail explain the effect of the design variables on the performance of the geometry and provide a more detailed evaluation on the improvements possible utilising CFD simulations and whether this knowledge can be effectively represented in an educational package for use within the SiS technology challenge.

References

- Bertram, V. (2019). Submarine Hull Design. [online] Ntnu.edu. <https://www.ntnu.edu/documents/20587845/1266707380/2012Chennai_SubmarineDesign.pdf/9bb180be-a08d-48ea-af4e-7e5e19210d3b>
- Bertram, V. (2012). Practical ship hydrodynamics, second edition. 2nd ed. Amsterdam: Elsevier.
- Friedman, N. (1984). Submarine design and development. Annapolis, Maryland: Naval Institute Press.
- Gertler, M. (1950). Resistance Experiments on a Systematic Series of Streamlined Bodies of Revolution-For Application to the Design of High-Speed Submarines. <Apps.dtic.mil. https://apps.dtic.mil/dtic/tr/fulltext/u2/a800144.pdf>
- Hervey, J. and Till, G. (1994). Submarines. London: Brassey.
- Joubert, P. (2004). Some Aspects of Submarine Design Part 1. Hydrodynamics. Archive.org. <https://archive.org/stream/DTIC_ADA428039/DTIC_ADA428039_djvu.txt>
- Mises, R. (2012). Theory of Flight. Dover Publications. <https://www.britannica.com/technology/submarine-naval-vessel>
- Moonesun, M., Mikhailovich, K., Tahvildarzade, D. and Javadi, M. (2014). Practical scaling method for underwater hydrodynamic model test of submarine. Journal of the Korean Society of Marine Engineering, 38(10), pp.1217-1224. <http://jkosme.or.kr/_PR/view/?aidx=3471&bidx=285>
- Moonesun, Mohammad & Javadi, Mehran & Charmdooz, Pejman & , Karol & Mikhailovich, Uri. (2013). Evaluation of submarine model test in towing tank and comparison with CFD and experimental formulas for fully submerged resistance. Indian Journal of Geo-Marine Sciences. 42. 1049-1056.
- REA (Re-Engineering Australia). (2019). 2019 Level 4 – Submarine Build Manual. < https://3ixa2917tenz3fyiar4esjdf-wpengine.netdna-ssl.com/wp-content/uploads/2019-SiS-Build-Manual.pdf>
- Renilson, M. (2015). Submarine Hydrodynamics. Launceston: Springer.

Appendix A: Details of the simulated three geometries

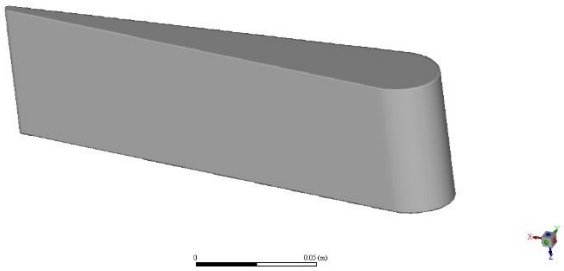

Figure 9: (a) Isometric view of geometry 1

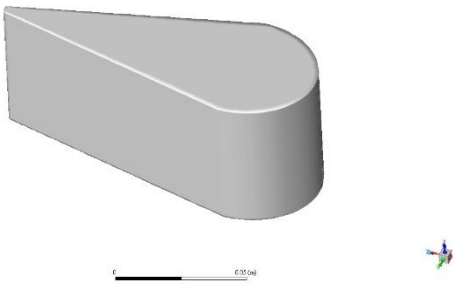

Figure 9: (b) Isometric view of geometry 2

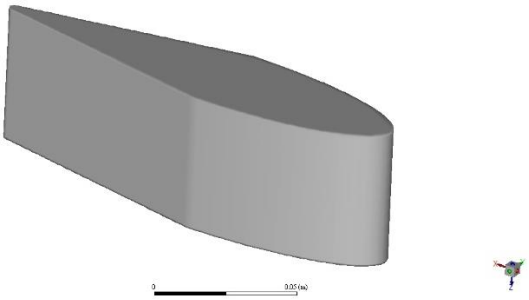

Figure 9: (c) Isometric view of geometry 3

Appendix B: Reynold's Number Calculations

$$Re = \rho VL/\mu$$

Equation 4. Reynold's number (Bertram, 2019).

Sail	Velocity (m/s)	Reynold's Number ()	Corresponding Air Speed (m/s)
1	0.75	149282.1535	10.90308104
1	1	199042.8714	14.53744139
1	1.25	248803.5892	18.17180174
2	0.75	94794.1675	10.90308104
2	1	126392.2233	14.53744139
2	1.25	157990.2792	18.17180174
3	0.75	118679.3121	10.90308104
3	1	158239.0828	14.53744139
3	1.25	197798.8534	18.17180174